Available online at www.sciencedirect.com
SCIENCE DIRECT®
Journal of the European Ceramic Society 25 (2005) 417–424
www.elsevier.com/locate/jeurceramsoc

Uniaxial viscosity of low-temperature cofired ceramic (LTCC) powder compacts determined by loading dilatometry

Rong-Jun Xie [a,b,*], Ruzhong Zuo [b], Emil Aulbach [b], Uwe Mackens [c], Naoto Hirosaki [a], Jürgen Rödel [b]

[a] *Advanced Materials Laboratory, National Institute for Materials Science (NIMS), Namiki 1-1, Tsukuba, Ibaraki 305-0044, Japan*
[b] *Institute of Materials Science, Darmstadt University of Technology, Petersenstr. 23, 64287 Darmstadt, Germany*
[c] *Philips Research Laboratories, Weißhausstraße 2, 52066 Aachen, Germany*

Received 15 November 2003; accepted 18 January 2004
Available online 2 June 2004

Abstract

This paper reports on the experimental determination of the uniaxial viscosity of two commercially available low-temperature cofired ceramic (LTCC) powder compacts, Ceramtape GC (glass-ceramic) and Ferro A6M (glass), by loading dilatometry. Isothermal sintering of cylindrical green compacts was carried out at temperatures ranging from 720 to 840 °C and under varying uniaxial compressive loads of 0–50 N (corresponding to 0–0.5 MPa). Both instantaneous radial and axial strains were measured during sintering. These data were analyzed by using constitutive laws for a porous sintering body and the uniaxial viscosity was calculated as a function of relative density. The activation energy for viscosity was independent of relative density and showed an average value of 668 ± 76 kJ/mol for the Ceramtape material but was not accessible for the Ferro material. The viscosity data were compared with several theoretical models.

Keywords: Dilatometry; Sintering; Porosity; Glass; Glass ceramics; LTCC

1. Introduction

Low-temperature cofired ceramic (LTCC) was developed as an advancement of thick film hybrid technology in the 1980s and has been significantly improved over the years.[1,2] Consumer applications of microwave devices, particularly high frequency and wireless communication devices, have grown rapidly in the last few years. These applications require packaging materials with high performance, high volume manufacturing capabilities and low cost. LTCC offers an ideal solution for these requirements.[3] It provides high reliability and the design flexibility to realize true 3D structure and to incorporate capacitive and resistive components within the hermetic structure.

LTCC technology demands cofiring of LTCC substrates and metal conductors or embedded electrical components. Mismatched densification kinetics of different materials would result in undesired defects, such as delamination, cracks, and warpage, in the final products.[4–9] For example, in the case of a double-layered structure ($d \ll D$) the camber rate is expressed as follows:[7–9]

$$\dot{\kappa} \approx -\left(\frac{6d}{D^2}\right)\left(\frac{1-\nu_p^C}{1-\nu_p^M}\right)\left(\frac{E_p^C}{E_p^M}\right)\Delta\dot{\varepsilon}^{C,M} \quad (1)$$

where d and D, ν_p^M and ν_p^C, E_p^M and E_p^C are the thickness, viscous Poisson's ratio and uniaxial viscosity of metal and ceramic plates, respectively. $\Delta\dot{\varepsilon}^{C,M}$ quantifies the difference in densification strain rate between the metal and ceramic plates. Since the viscous Poisson's ratio varies little with density,[10,11] the above equation indicates that the camber rate mainly depends on the uniaxial viscosity and densification strain rate differential. To predict the curvature development, it is of importance to know how the uniaxial viscosity and differential strain rate are affected by relative density (or porosity) in a sintering body. The primary objective of the present study was thus to determine the uniaxial viscosity of LTCC materials as a function of relative density experimentally.

* Corresponding author. Tel.: +81-29-860-4312; fax: +81-29-851-3613.
E-mail address: xie.rong-jun@nims.go.jp (R.-J. Xie).

0955-2219/$ – see front matter © 2004 Elsevier Ltd. All rights reserved.
doi:10.1016/j.jeurceramsoc.2004.01.022

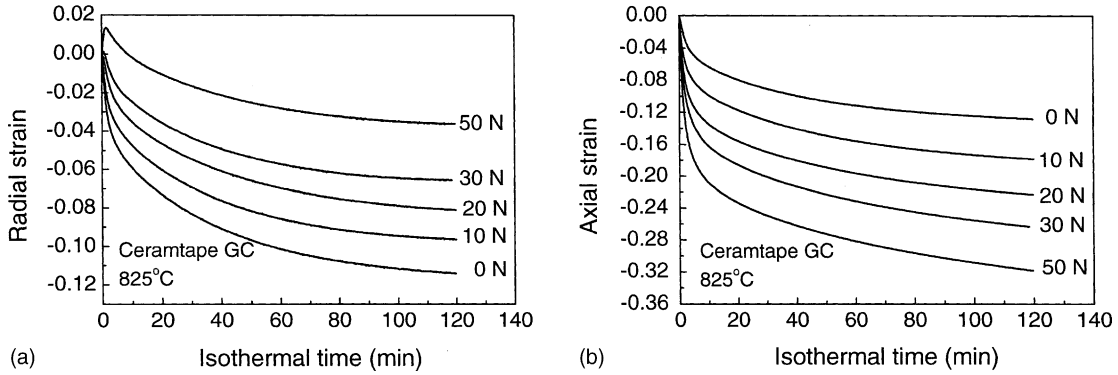

Fig. 1. (a) Radial and (b) axial strains as a function of isothermal time for the CT powder compacts sinter-forged at 825 °C under various loads.

So far, extensive efforts have been carried out in order to determine the viscosity of a sintering body, and several models have been presented.[10,12–18] Experimental techniques have also been used to determine the viscosity of a sintering body as a function of relative density, including loading dilatometry[15,16,19–25] and optical dilatometry.[26] Among these methods, sinter-forging types of experiment are considered as a common approach, where a uniaxial load is applied on the cylindrical powder compact and, radial and axial strains are measured simultaneously. The viscosity determination depends strongly on the accurate measurement of sintering strains which are converted to strain rates, hence a sinter-forging facility with high resolution is required in principle. A new loading dilatometer has been built up for sinter-forging experiments in our group, which is described in detail elsewhere.[21,27] The system mainly consists of a programmable heating furnace, a screw-driven loading frame and two high-resolution laser scanners for the simultaneous measurement of radial and axial strains with a resolution of ~2 μm. The loading unit (Instron model 5565) has a fast response so that an accurately controllable uniaxial force (±0.1 N) can be loaded on the specimen.

In this paper, this newly-developed loading dilatometer was utilized to measure the instantaneous radial and axial strains during isothermal sintering under varying uniaxial compressive loads for LTCC materials. The data were analyzed using constitutive laws and the uniaxial viscosity was computed as functions of relative density and temperature. The experimentally determined uniaxial viscosity was also compared to several theoretical predictions.

2. Experimental procedure

Two commercially available LTCC material tapes were used in this study: Ceramtape GC (abbreviated as "CT", CeramTec AG, Plochingen, Germany) and Ferro A6M (abbreviated as "FA", Ferro Corporation, Ohio, USA). The CT material is a glass-ceramic, which consists of Al_2O_3 and anorthite glass (55–70 vol.%), with the Al_2O_3 particle size of 1.0–1.5 μm. The FA material is a crystallizable wallostonite glass which mainly contains CaO, SiO_2, and B_2O_3 and has a softening point of 700 °C. The LTCC powders were obtained by firing the LTCC tapes at 400 °C for 2 h with a heating rate of 5 °C/min. Cylindrical powder compacts were then prepared by cold pressing under a uniaxial stress of 50 MPa, followed by cold isostatic pressing under 700 MPa. The green products have a final dimension of ~20 mm in height and ~11 mm in diameter, and the green density is 65.4 ± 0.3% and 68.7 ± 0.8% of theoretical density for the CT and FA samples, respectively.

Sinter-forging was performed in air. Samples were separated from the pushrods by alumina disks, which were coated with boron nitride (BN) powder to reduce the friction

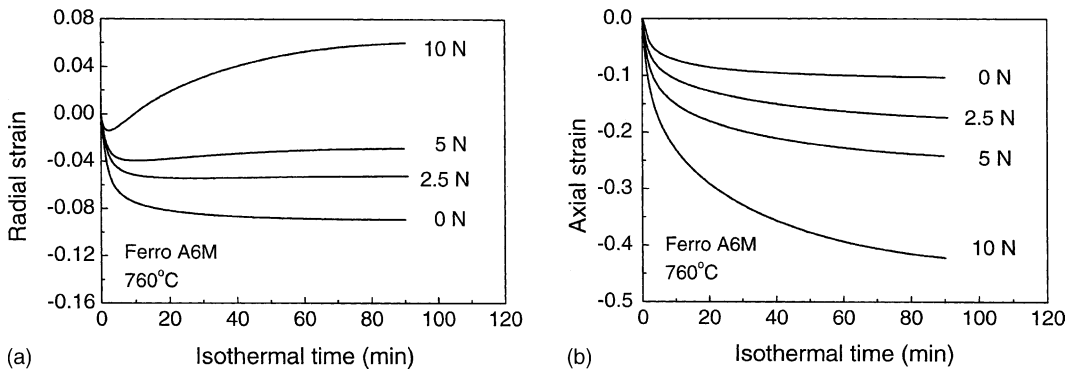

Fig. 2. (a) Radial and (b) axial strains as a function of isothermal time for the FA powder compacts sinter-forged at 760 °C under various loads.

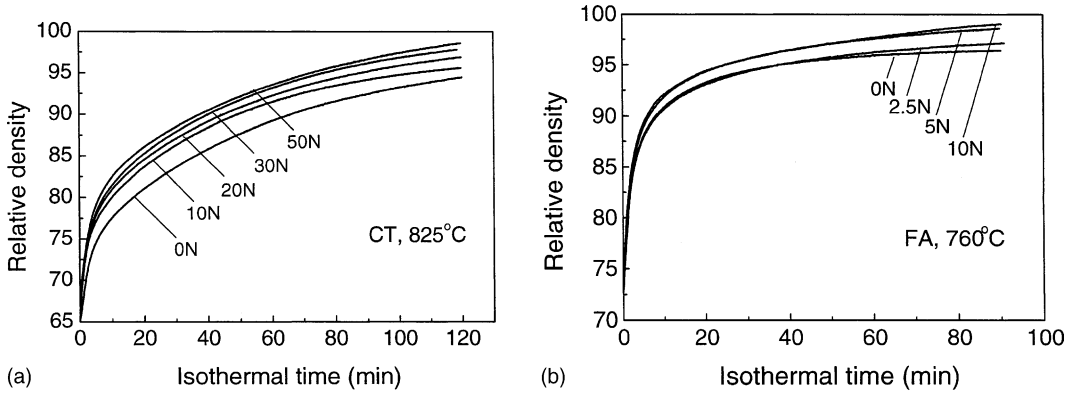

Fig. 3. Relative density as a function of isothermal time for (a) CT and (b) FA powder compacts.

between the sample and the disks and thus to minimize the barreling. Isothermal sintering was conducted at 775–840 °C for CT and 700–740 °C for FA under simple uniaxial compressive loads of 0–50 N (corresponding to 0–0.5 MPa compressive stress), with a heating rate of 30 °C/min. The temperature was monitored using a thermocouple that is placed close to the specimen. The samples were held at 650 °C for 10 min to achieve thermal equilibrium. The constant load was applied immediately as the desired temperature was reached. As the experiments terminated, the load was released and the electrical power was turned off, allowing the sample to cool down in the furnace.

A FA specimens sintered at 760 °C under 5 N was analyzed by X-ray diffraction (XRD; Philips PW1700), operating at 40 kV and 40 mA and using Cu Kα radiation (λ = 1.5406 Å). Differential thermal analysis (DTA) was performed in air on samples with a weight of approximately 65 mg, using Bähr DTA 701 (Bähr-Thermoanalyse GmbH, D-32609 Hüllhorst, Germany). The heating rate was 5 °C/min.

3. Data analysis

Assuming that a porous sintering body is isotropic and using the elastic-viscous analogy, Scherer[13] proposed the following constitutive equations to describe the response of a viscous porous body to external constraints during sintering:

$$\dot{\varepsilon}_r = \dot{\varepsilon}_f + E_p^{-1}[\sigma_r - \nu_p(\sigma_\theta + \sigma_z)] \quad (2a)$$

$$\dot{\varepsilon}_z = \dot{\varepsilon}_f + E_p^{-1}[\sigma_z - \nu_p(\sigma_r + \sigma_\theta)] \quad (2b)$$

where σ_r, σ_θ, and σ_z are the radial, hoop and axial stresses; $\dot{\varepsilon}_f$, strain rate of a free sample (i.e., no external stress is applied); $\dot{\varepsilon}_r$ and $\dot{\varepsilon}_z$, radial and axial strain rates; E_p, uniaxial viscosity and ν_p is the viscous Poisson's ratio of the porous sintering body.

$$\dot{\varepsilon}_z = \dot{\varepsilon}_f + \frac{1}{E_p}\sigma_z \quad (3)$$

Further, the expression for E_p can be deduced from the above equation

$$E_p = \frac{\sigma_z}{\dot{\varepsilon}_z - \dot{\varepsilon}_f} \quad (4)$$

Eq. (4) then is the key equation we will utilize in our evaluations. We will computer the uniaxial viscosity using measurements of the axial strain rate at a given uniaxial stress and the free strain rate compared at the same density. The radial strain is only required for the instantaneous computation of density. Therefore, complications, which may arise from an initially anisotropic microstructure or a possible

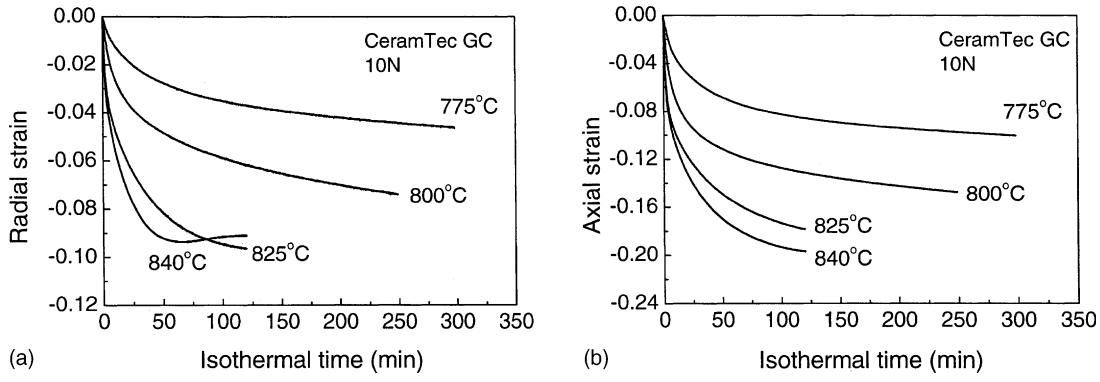

Fig. 4. (a) Radial and (b) axial strains as a function of isothermal time for the CT powder compacts sinter-forged at varying temperatures under 10 N.

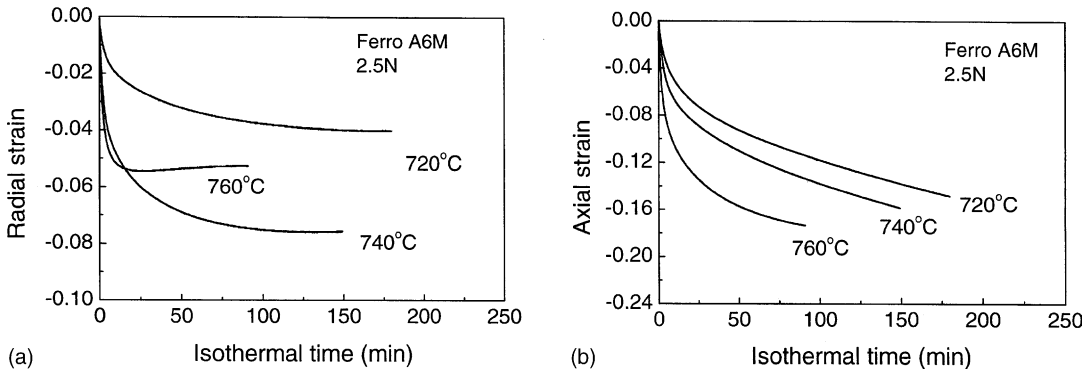

Fig. 5. (a) Radial and (b) axial strains as a function of isothermal time for the FA powder compacts sinter-forged at varying temperatures under 2.5 N.

evolution of an anisotropic microstructure as described by Zuo et al.[23] in alumina are circumvented.

The experiment gives data for the changes in the length and diameter of the specimen with time. Since the specimen undergoes large deformation, the measured data are converted to true strain rather than engineering strain. If the time-dependent length and diameter for the specimen are given by $L(t)$ and $2R(t)$, then the equations for axial and radial strains may be written as

$$\varepsilon_z = \ln \frac{L(t)}{L(0)} \tag{5a}$$

$$\varepsilon_r = \ln \frac{R(t)}{R(0)} \tag{5b}$$

The densification strain or volumetric strain $\dot{\rho}/\rho = \varepsilon_v$ is obtained from ε_r and ε_z using following equation:[28]

$$\varepsilon_v = 2\varepsilon_r + \varepsilon_z \tag{6}$$

The change of density during sintering is related to ε_v by Eq. (7)

$$\rho = \rho_g \exp(|\varepsilon_v|) \tag{7}$$

where ρ_g is the initial relative density of the powder compact measured at the onset of isothermal sintering by the volumetric method.

The applied axial load, F, is kept constant during sintering. Since the cross-sectional area of the specimen, $A(=\pi R^2)$, changes with time, the axial stress σ_z is a function of time. The time-dependent axial stress can be calculated from the radial strain using the following equation:

$$\sigma_z = \frac{F}{\pi R(0)^2} \exp(-2\varepsilon_r) \tag{8}$$

4. Results and discussion

4.1. Sinter-forging curves

The instantaneous axial and radial displacements are measured during sintering, and then the corresponding radial and axial strains are calculated from Eq. (5). It is observed that the radial strain is less than 1.0% larger than the axial strain during sintering without loads (i.e., free sintering), indicating slight anisotropy in shrinkage which may be due to the irregular morphology of the particle and the presence of glassy phase. The anisotropic shrinkage becomes remarkable with the application of compressive loads, but in this case the axial strain is larger than the radial one.

4.1.1. Effect of load

Figs. 1 and 2 present the curves for time-dependent radial and axial strains (ε–t curve) of the CT and FA powder compacts sintered at 825 and 760 °C under different values of axial loads, respectively. A load of 1 N represents an

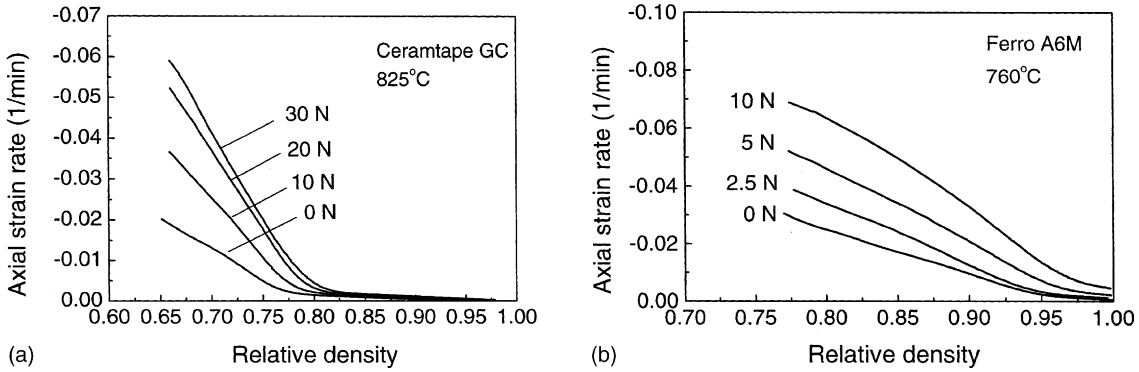

Fig. 6. The axial strain rate as a function of relative density for (a) CT and (b) FA powder compacts.

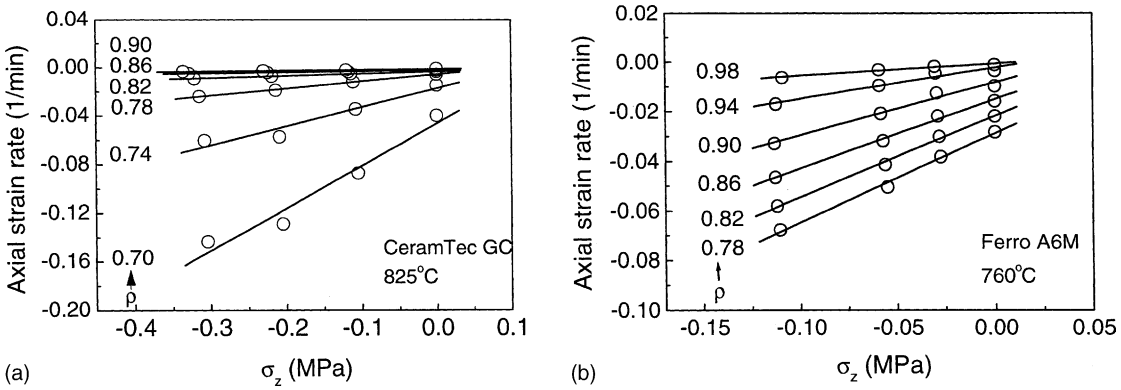

Fig. 7. The axial strain rate as a function of applied stress for (a) CT and (b) FA powder compacts.

initial stress of about 10 kPa, and $t = 0$ represents the onset of isothermal sintering. As seen, the axial strain is always negative and increases as the compressive stress increases for both samples. The radial strain is negative at low stresses but positive (more apparent for the FA sample) at large stresses. Salamone et al.[24] has addressed that it is due to Poisson's expansion in the radial dimension as a result of a compressive axial stress. Venkatachari[30] has explained that deformation strain dominates when the applied compressive stress is large enough, which leads to a positive value of the radial strain. Moreover, the critical stress at which the radial strain is positive is different for both materials, which is probably dependent on the sintering stress. The sintering stress of the FA material is lower than that of the CT material (unpublished research[29]); therefore, the critical stress is smaller for the FA material.

Fig. 3 shows the effect of the applied compressive stress on the relative density of CT and FA powder compacts sintered at 825 and 760 °C, respectively. Note that the applied stress generally improves the densification for both materials, notably for the CT sample. The driving force for densification includes intrinsic sintering stress (Σ) and applied uniaxial stress (σ_z), which can be presented in the equation as follows:[16,30]

$$\frac{\dot{\rho}}{\rho} = \frac{\Sigma + (1/3)|\sigma_z|}{K_p} \tag{9}$$

where K_p is bulk viscosity. The maximum hydrostatic sintering stress is approximately −0.25 MPa for CT samples and approximately −0.11 MPa for FA samples[29], respectively, hence the applied stress is in the order of the sintering stress in this work. This implies that the applied stress has a significant effect on the densification rate.

4.1.2. Effect of temperature

The effect of temperature on axial and radial strains is shown in Figs. 4 and 5 for the CT and FA powder compacts, respectively. Note that both the radial and axial strains increase as the sintering temperature rises. At higher temperatures, the radial strain reduces after a certain period of time, indicating that the deformation strain dominates.

4.2. Axial strain rate

The axial strain rate is obtained by fitting smooth curves to the data points of the ε_z–t curves, followed by differentiating with respect to time. The results are shown in Fig. 6 as a function of relative density for samples sintered at 825 (CT)

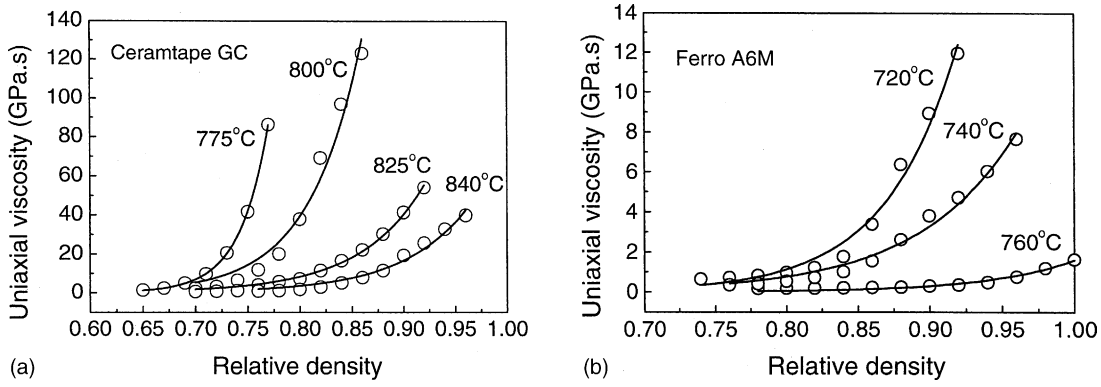

Fig. 8. The uniaxial viscosity as a function of relative density for (a) CT and (b) FA powder compacts.

and 760 °C (FA) under various loads. Note that under each load the axial strain rate drops rapidly in the early stages of densification, and then declines gradually in the intermediate and final stages.

Fig. 7 provides the axial strain rate as a function of applied stress for CT (825 °C) and FA (760 °C) samples in a wide density range. The stress value is obtained from Eq. (8), considering the change in the cross-sectional area of the specimen during sintering. In the stress level of interest, a linear relationship between the axial strain rate and stress is evident over the entire density range.

4.3. Uniaxial viscosity E_p and activation energy Q_η

The uniaxial viscosity, E_p, is obtained from the slope of $\dot{\varepsilon}_z - \sigma_z$ curves at a given density according to Eq. (3). Fig. 8 displays the uniaxial viscosity as a function of relative density for both LTCC powder compacts, which are sintered at different temperatures. The results clearly show that the uniaxial viscosity varies in a non-linear fashion with relative density. At a given temperature, E_p increases slightly with increasing density in the low-density region, and goes up sharply in the high-density region. This behavior is also seen in other materials.[15,23] Low E_p values observed in the low-density region are attributed to small necks between particles and thus a small load-bearing area. As densification proceeds, the inter-particle necking develops and the load-bearing area increases so that E_p increases rapidly.

The activation energy for viscosity, Q_η, can be determined from the Arrhenius plots. Plotted in Fig. 9 are $\ln(E_p) - 1/T$ curves at densities ranging from 72 to 84% for the CT material. As seen, these curves are linear and the straight lines are nearly parallel to each other, suggesting that the activation energy of viscosity is nearly independent on density for the CT sample. The average Q_η value is 668 ± 76 kJ/mol over the entire density range. Based on the results of Figs. 8 and 9, the uniaxial viscosity for the CT material can be reasonably well represented by Eq. (10)

$$E_p = f(\rho)\, e^{Q_\eta/RT} \tag{10}$$

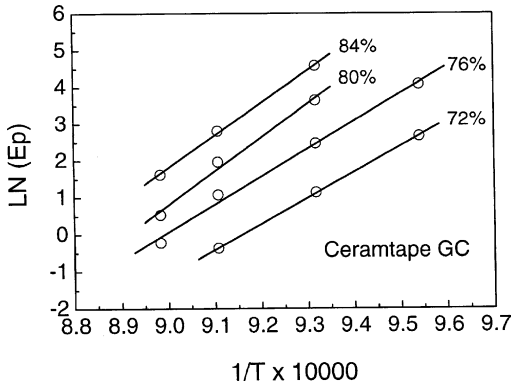

Fig. 9. Arrenhnuis plots ($\ln(E_p) \sim 1/T$) of CT powder compacts.

For the FA material, the activation energy for viscosity is not accessible. Chemical reactions among initial components (i.e., CaO, B_2O_3, SiO_2, and etc.) in the glass powder occur at 760 °C, forming crystalline phases of mainly $CaSiO_3$ and CaB_2O_4 in the sintered material as seen in Fig. 10a. The result of DTA data, as shown in Fig. 10b, confirms the above finding. Four exothermic peaks are clearly seen in the DTA curve, which are identified at 330, 410, 825, and 850 °C, respectively. The first two peaks are due to the thermal decomposition of the binder system, and the last two are attributed to the crystallization of glass. Besides these four peaks there is a shoulder beginning at 750 °C, indicating the onset of crystallization. This is in agreement with the limited degree of crystallization at 760 °C as can be observed in Fig. 10a. At temperatures below 750 °C no chemical reactions occur. Therefore, it can be expected that the FA material is still in the glassy state when sintered below 750 °C while begins to crystallize when sintered above 750 °C. Therefore, the activation energy for viscosity is different for these two temperature regimes and is more complex in the high temperature regime (e.g., the amount of crystalline phase changes during sintering). Hence, more experimental data of viscosity and phase content at higher temperatures are needed to determine the activation energy for viscosity.

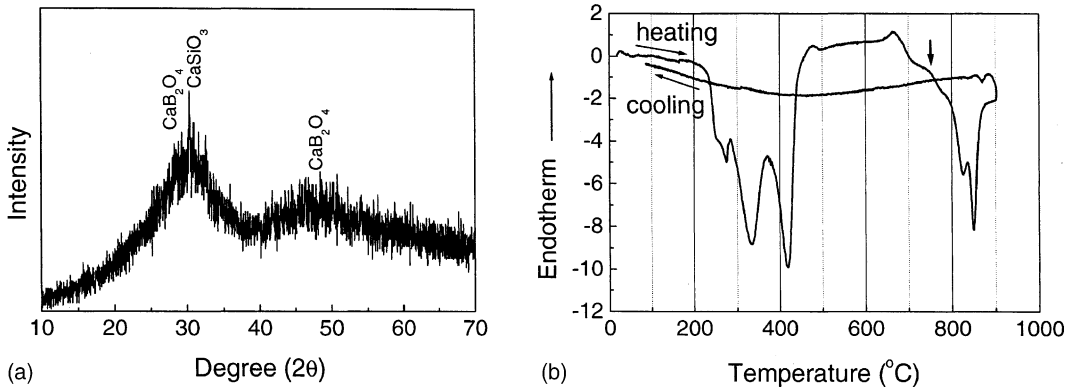

Fig. 10. (a) XRD pattern of the FA compact sinter-forged at 760 °C under 5 N, showing the crystalline phases of $CaSiO_3$ and CaB_2O_4 and (b) DTA data of the FA tape upon heating and cooling, indicating the onset of crystallization at 750 °C.

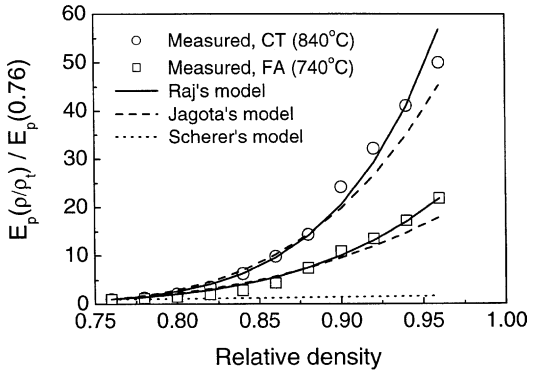

Fig. 11. Normalized uniaxial viscosity $E_p(\rho/\rho_t)/E_p(0.76)$ as a function of relative density for CT and FA powder compacts. The experimental data are compared with models by Scherer[13], Raj[16], and Jagota[31].

4.4. Comparison of experimental results and models

As mentioned previously, a number of models have been proposed to describe the viscosity-density relation. For comparison, the uniaxial viscosity is normalized by the value at the onset of isothermal sintering (i.e., at $\rho/\rho_t = 0.76$) in order to eliminate the effect of initial particle size. Thus, the normalized uniaxial viscosity is defined as

$$\bar{E}_p = \frac{E_p(\rho/\rho_t)}{E_p(0.76)} \tag{11}$$

Comparison of measured viscosities with several models is plotted in Fig. 11. The values of a in Raj's model[16] and pu in Jagota's model[31] were fitted to the experimental results at $\rho/\rho_t = 0.88$. Although Scherer developed his model for sintering of viscous materials, which should be applicable to our materials, the measured viscosity data failed to agree with his prediction, typically in the high-density region. One possible reason for this failure is that spherical pore morphology is assumed and does not change during sintering in Scherer's model. In fact, both pore shape and concentration change during sintering.[19,30] Both Raj and Jagota's models provide a reasonable empirical fit to our data over the entire density region.

5. Conclusions

Two types of LTCC powder compacts were sintered at varying temperatures and under various uniaxial compressive loads. Measurement of both the axial and radial strains led to a description of time-dependent relative density and strain rates. These data were analyzed based on the constitutive models for a sintering body and, the obtained results are summarized as follows:

(1) Sinter-forging types of experiment can be used to determine the constitutive parameter, uniaxial viscosity E_p, as a function of relative density.
(2) For both materials, the uniaxial viscosity changed non-linearly with relative density, starting from a very low value in the low-density region and increasing rapidly after a threshold density.
(3) The viscosity data were compared with several theoretical predictions, and agreed well with models by Raj and Jogata.
(4) The activation energy for viscosity Q_η was computed from the Arrhenius plots for the CT material. Q_η was found to be invariant with relative density at 668 ± 76 kJ/mol.

Acknowledgements

The authors would like to thank the Alexander von Humboldt (AvH) Foundation (Germany) for a research fellowship for one of us (R.-J. Xie). Donation of CT samples by CeramTec AG (Plochingen, Germany) is greatly appreciated.

References

1. Tummala, R. R., Ceramics and glass-ceramic packaging in the 1990s. *J. Am. Ceram. Soc.* 1991, **74**, 895–908.
2. Brown, R. L., Shapiro, A. A. and Polinski, P. W., The integration of passive components into MCMs using advanced low-temperature cofired ceramics. *Int. J. Microcircuits Electron. Packag.* 1993, **16**, 328–338.
3. Russer, P. and Vietzorreck, L., New millimeterwave technologies for communications and sensorics. *Frequenz* 2003, **57**, 38–44.
4. Bordia, R. K. and Raj, R., Sintering behavior of ceramic films constrained by a rigid substrate. *J. Am. Ceram. Soc.* 1985, **68**, 287–292.
5. Cheng, T. and Raj, R., Flaw generation during constrained sintering of metal–ceramic and metal–glass multilayer films. *J. Am. Ceram. Soc.* 1989, **72**, 1649–1655.
6. Kumar, A. H. and Tummala, R. R., State-of-the art, glass-ceramic/copper, multilayer substrate for high performance computers. *Int. J. Hybrid Microelectron.* 1991, **14**, 137–150.
7. Lu, G. Q., Sutterlin, R. C. and Gupta, T. K., Effect of mismatched sintering kinetics on camber in a low temperature cofired ceramic package. *J. Am. Ceram. Soc.* 1993, **76**, 1907–1914.
8. Jean, J. H. and Chang, C.-R., Camber development during cofiring Ag-based low-dielectric-constant ceramic package. *J. Mater. Res.* 1997, **12**, 2743–2750.
9. Jean, J. H. and Chang, C.-R., Cofiring kinetics and mechanism of an Ag-metallized ceramic-filled glass electronic package. *J. Am. Ceram. Soc.* 1997, **80**, 3084–3092.
10. Bordia, R. K. and Scherer, G. W., On constrained sintering-II. Comparison of constitutive models. *Acta Mater.* 1988, **36**, 2399–2409.
11. Zuo, R., Aulbach, E. and Rödel, J., Viscous Poisson's coefficient determined by discontinous hot forging. *J. Mater. Res.* 2003, **18**, 2170–2176.
12. Olevsky, E. A., Theory of sintering: from discrete to continuum. *Mater. Sci. Eng. R* 1998, **23**, 41–100.
13. Scherer, G. W., Sintering inhomogeneous glasses: application to optical waveguides. *J. Non-Cryst. Solids* 1979, **34**, 239–256.
14. Hsueh, C. H., Evans, A. G., Cannon, R. M. and Brook, R. J., Viscoelastic stresses and sintering damage in heterogeneous powder compacts. *Acta Metall.* 1986, **34**, 927–936.
15. Rahaman, M. N., De Jonge, L. C. and Brook, R. J., Effect of shear stress on sintering. *J. Am. Ceram. Soc.* 1986, **69**, 53–58.

16. Ducamp, V. C. and Raj, R., Shear and densification of glass powder compacts. *J. Am. Ceram. Soc*. 1989, **72**, 798–804.
17. Sura, V. M. and Panda, P. C., Viscosity of porous glass. *J. Am. Ceram. Soc.* 1990, **73**, 2697–2701.
18. Jagota, A. and Scherer, G. W., Viscosities and sintering rates of composites packings of spheres. *J. Am. Ceram. Soc*. 1995, **78**, 521–528.
19. Rahaman, M. N., De Jonghe, L. C., Scherer, G. W. and Brook, R. J., Creep and densification during sintering of glass powder compacts. *J. Am. Ceram. Soc.* 1987, **70**, 766–774.
20. Rahaman, M. N. and De Jonghe, L. C., Sintering of spherical glass powder under a uniaxial stress. *J. Am. Ceram. Soc*. 1990, **73**, 707–712.
21. Cai, P. Z., Messing, G. L. and Green, D. L., Determination of the mechanical response of sintering compacts by cyclic loading dilatometry. *J. Am. Ceram. Soc*. 1997, **80**, 445–452.
22. Gillia, O., Josserond, C. and Bouvard, D., Viscosity of WC–Co compacts during sintering. *Acta Mater.* 2001, **49**, 1413–1420.
23. Zuo, R., Aulbach, E., Bordia, R. K. and Rödel, J., Critical evaluation of hot forging experiments: case study in alumina. *J. Am. Ceram. Soc.* 2003, **86**, 1099–1105.
24. Salamone, S. M., Stearn, L. C., Bordia, R. K. and Harmer, M. P., Effect of rigid inclusions on the densification and constitutive parameters of liquid phase sintered $YBa_2Cu_3O_{6+x}$ powder. *J. Am. Ceram. Soc.* 2003, **86**, 883–892.
25. Zuo, R., Aulbach, E. and Rödel, J., Experimental determination of sintering stresses and sintering viscosities. *Acta Mater.* 2003, **51**, 4563–4574.
26. Bang, J., Lu, G. Q. and Calata, J. N., Determination of shear viscosity of borosilicate glass + silica powder compacts by an optical system. *J. Mater. Res.* 1999, **14**, 1062–1068.
27. Aulbach, E., Zuo, R. and Rödel, J., Laser-assisted high resolution loading dilatometer and applications. *Exp. Mech.* 2004, **44**, 2170–2176.
28. Raj, R., Separation of cavitation-strain and creep-strain during deformation. *J. Am. Ceram. Soc.* 1982, **65**, c-46.
29. Xie, R. -J. *et al.*, unpublished work.
30. Venkatachari, K. R. and Raj, R., Shear deformation and densification of powder compacts. *J. Am. Ceram. Soc*. 1986, **69**, 499–506.
31. Jagota, A., Mikeska, K. R. and Bordia, R. K., Isotropic constitute model for sintering particle packings. *J. Am. Ceram. Soc.* 1990, **73**, 2266–2273.